Title: Loss of Aurora kinase signaling allows lung cancer cells to adopt an alternative cell cycle and resist anti-mitotic drugs.

Author list: Vural Tagal[1], Michael G. Roth[1,2,3]

Affiliations: Departments of Biochemistry[1], Harold Simmons Comprehensive Cancer Center[2], UT Southwestern Medical Center, Dallas TX 75390 USA

Corresponding authors

Lead contact[3]: Michael G. Roth michael.roth@utsouthwestern.edu

Abstract

Drug resistance is a major challenge for cancer medicine and, despite substantial research, our understanding of the molecular determinants of drug resistance mechanisms remains incomplete. In the course of investigating vulnerabilities of non-small cell lung cancer to Aurora kinase inhibitors, we discovered that some cancer cells continue to grow after the inhibition of Aurora kinase signaling by switching to a cell cycle variant, a form of endocycle, that avoids mitosis and continues to replicate DNA without dividing. Such cells are completely resistant to treatment with antimitotic drugs as long as Aurora kinases are inhibited. These cancer "persister" cells can re-enter the proliferative cell cycle when anti-mitotic treatment is terminated. Endocycling, which occurs naturally in specialized cell types in many species, can also be used by cancer cells to survive anti-mitotic cancer drugs.

Introduction

A subpopulation of cancer cells often remains alive even after successful therapy has eliminated most tumor cells. Those surviving cancer cells are the prime source for recurring tumors and the ultimate failure of therapy. Therefore, understanding the mechanisms that allow therapy-tolerant cancer "persister" cells is fundamental for developing strategies to defeat drug resistance.

Most cancers tend to be heterogenous and genetically plastic, as they frequently express transcriptional pathways normally not active in their original cell types (Hanahan and Weinberg, 2011; Simpson et al., 2005; Zhang et al., 2018). The tumor population as a whole has the potential to access all the cellular mechanisms encoded in the genome and drug treatment will select for those cells that happen to have adopted an escape mechanism. Well-known examples of drug resistance strategies to traditional chemotherapies include upregulating efflux pumps or drug metabolizing enzymes. Recently, more specific mechanisms for surviving newer, more selective therapies have been observed. These include mutations in drug targets that prevent drug binding (Janne, 2008; Pao et al., 2005) but perhaps more commonly the adoption of alternative, or "by-pass" mechanisms. For example, Hangauer et al. (2017) and Viswanathan et al. (2017) demonstrated that in response to anti-RTK therapy, persisting cancer cells have switched to a GPX4-dependent state and survive until anti-RTK therapy has ended. As therapeutics become more selective and "personalized" to target specific vulnerabilities in a tumor, such more specific resistance mechanisms can be expected.

Currently, anti-mitotic drugs represent a major class of cancer medicines. This class includes microtubule-stabilizing drugs, such as paclitaxel and docetaxel, and destabilizing agents, such as vinorelbine and vinblastine (Steinmetz and Prota, 2018). More recently agents that target the kinases that regulate mitotic spindle formation and timing, such as Aurora and Polo-like kinases, have entered clinical trials (Otto and Sicinski, 2017; Steinmetz and Prota, 2018).

In the course of studying hypersensitivity to inhibitors of Aurora kinase A (Tagal et al., 2017), we reported an unusual dose response relationship to Aurora kinase inhibitors. In some non-small cell lung cancer (NSCLC) lines, more cells survived the inhibitor treatment at high than

at lower drug concentrations. Survival of a small remnant population after treatment with anti-mitotic drugs is a common observation. A prominent current explanation for this cell population is called “mitotic slippage” (Sinha et al., 2019). This concept assumes that some cells manage to struggle through mitosis without triggering an apoptotic response and subsequently either leave the proliferative cell cycle or continue to “slip” through it.

However, alternative cell cycles are normally used for the production of particular cell types and tissues such as megakaryocytes, placental trophoblasts or hepatocytes in mammals (Edgar et al., 2014; Gupta, 2000; MacAuley et al., 1998; Ravid et al., 2002). This class of alternative cell cycles, which do not require a mitotic machinery, could provide a survival mechanism by avoiding the catastrophic consequences of anti-mitotic perturbagens. We show in the work presented below that many NSCLC cell lines grow by adopting an endocycle when Aurora kinases are inhibited. However, unlike normal cells for which endocycles are part of terminal differentiation, a subset of endocycling NSCLC cells can re-enter the proliferative cell cycle after Aurora kinase inhibitors are withdrawn.

Results

Aurora kinase A is an important regulator of mitosis and functions in the assembly of the mitotic spindle (Bury et al., 2017; Gopalan et al., 1997; Hannak et al., 2001). Several different Aurora A inhibitors have been developed and are currently in clinical trials as anti-cancer drug candidates (Otto and Sicinski, 2017). In a previous study, we investigated these inhibitors and observed an unusual drug response relationship with an Aurora kinase A inhibitor, MLN8237/Alisertib (MLN8237 henceforth) (Tagal et al., 2017). In contrast to the standard sigmoidal or monophasic dose-response phenotypes (Figure 1A, C), a subgroup of cell lines treated with MLN8237 exhibited a multiphasic “camelback” drug-response pattern (Figure 1E). VX-689, another Aurora kinase A inhibitor, also caused a similar response pattern in the same panel of non-small cell lung cancer (NSCLC) lines (Figure 1B, D, F). This unexpected drug response pattern of increased cell survival at higher drug concentrations suggested that secondary targets of these inhibitors might control a mechanism leading to drug resistance. This would be of concern, since peak plasma concentrations of MLN8237 in humans reach 3 μM, well above the concentration at which it selectively inhibits its primary target (Cervantes et al., 2012). Thus, it was of interest to identify the secondary targets of Aurora A inhibitors and the respective drug resistance mechanism.

NSCLC line NCI-H1693 was selected as representative of cell lines capable of this unusual dose-response because it had the most dramatic phenotype with 35% of the cells growing at 87% of the rate of an untreated population in the presence of higher, potentially non-selective concentrations of MLN8237 (Figure 2A). NCI-H1693 cells had a first phase EC50 of 23 nM for MLN8237 and 64 nM for VX-689 (Figure 2A, C). The EC50s of MLN8237 and VX-689 for the second, “restorative” phase in which the viability increased, was 180 nM and 26 μM, respectively. At the highest and clinically irrelevant concentrations (Phase 3), MLN8237 gains a “general toxin” characteristic, which was not investigated in this study. In parallel, we measured Caspase 3/7 activity to determine if apoptotic cell death occurred in the presence of MLN8237 and VX-689 at any of concentrations measured. Apoptosis was first significantly detected at 16 nM for MLN8237 and 47 nM for VX-689. However, caspase activation was not detected during the second phase of the response to each drug (Figure

2B, D). In an orthogonal assay for cell growth, NCI-H1693 cells were stained with crystal violet after seven days treatment with either MLN8237 or VX-689 and cell densities were compared with the density of cells stained on day 0. We found that growth of NCI-H1693 cells was inhibited at Aurora A-selective concentrations and was restored at 410 nM and 33.3 μM of MLN8237 and VX-689, respectively (Figure 2E, G). Thus, the second phase of response to these two inhibitors not only helped NCI-H1693 cells survive, but also restored their growth.

Kinase inhibitors frequently are selective for their intended target only over a narrow concentration range (Bain et al., 2003; Bain et al., 2007; Davies et al., 2000). Aurora kinases B and C are two orthologues of Aurora A in humans and their high degree of homology is a well-known challenge for creating inhibitors specific to Aurora kinase A. Therefore, Aurora B and Aurora C were obvious candidates for the proteins responsible for reversing cytotoxic effects at higher concentrations of Aurora A inhibitors. Aurora kinases auto-phosphorylate when bound to their activators and their phosphorylation levels directly indicate their activation status in cells. In addition, Histone H3 is a well-characterized substrate of Aurora kinases B and C, and its phosphorylation at Serine 10 is established to be a direct marker of Aurora B or C activity (Bolton et al., 2002; Crosio et al., 2002; Giet and Glover, 2001; Walter et al., 2000). For these reasons, the phosphorylation statuses of Aurora kinases A, B, C and Histone H3 were measured 48 hours after treating NCI-H1693 cells with MLN8237 or VX-689 at a series of concentrations covering their two distinct phases of response. In these experiments, Paclitaxel at its EC100 (20 nM) was used as a positive control to inhibit the cell cycle at the mitotic stage where Aurora kinases are active. We observed increased phosphorylation of Aurora B and C, and Histone H3 starting at concentrations 50 nM of MLN8237 and 140 nM of VX-689. However, starting at 410 nM of MLN8237 and 33.3 μM of VX-689, phosphorylation of Aurora B and C, and Histone H3 was completely undetectable (Figures 2F, H). Thus, there was a precise overlap between cell death, apoptosis and selective inhibition of Aurora A and between lack of apoptosis, continued cell growth and inhibition of Aurora B and C (Figures 2I, J).

To test the hypothesis that Aurora B and C are the secondary targets causing the generation of cancer persister cells, we used two selective Aurora B and C inhibitors, AZD1152/Barasertib (AZD1152 henceforth) and GSK1070916 (Anderson et al., 2009; Mortlock et al., 2007). We first verified their selectivity for Aurora B and C compared to Aurora A by measuring auto-phosphorylation levels of Aurora kinases A, B and C, and phosphorylation of Histone H3 in NCI-H1693 cells. Paclitaxel at its EC100 was used as a positive control. At 50 nM AZD1152 or 15 nM GSK1070916 auto-phosphorylation of Aurora B, C and Histone H3, was not detected; but Aurora A was phosphorylated (Figure 3A, B). This indicated that at those concentrations, NCI-H1693 cells were arrested in mitosis at a point after activation of Aurora A. However, starting at 1.23 μM for AZD1152 or 140 nM for GSK1070916, phosphorylation of Aurora A was not detected, indicating that both drugs also inhibit Aurora A at higher concentrations.

The dose-response pattern of viability of NCI-H1693 cells to AZD1152 and GSK1070916 resembled the multiphasic “camelback" response of those cells to Aurora A selective inhibitors MLN8237 and VX-689 (Figure 3C-F). AZD1152 and GSK1070916 each caused significant reduction in viability of NCI-H1693 cells at concentrations selective for Aurora B

and C. However, growth was restored when NCI-H1693 cells were treated with concentrations above 1.23 μM and 140 nM of AZD1152 and GSK1070916, respectively (Figure 3G-H), where they began to antagonize Aurora A as a secondary target. These data suggested that inhibiting Aurora A or Aurora B and C activities alone caused significant mitotic catastrophe leading to cytotoxicity; but inhibition of all three Aurora kinases together did not (Figures 3I, J).

To ensure that Aurora kinases A, B and C, but not a previously unrecognized fourth target, are solely responsible of restoring viability induced with individual treatments of each of these four inhibitors, we treated NCI-H1693 cells with these four inhibitors as doublet combinations at concentrations where they are selective for their primary targets (Figure 4A, B). Combination therapy of Aurora A and Aurora B, C inhibitors did not cause additive or synergistic cytotoxicity; but instead allowed cell survival and growth (Figure 4C, E). We measured the activities of Caspase 3/7 (Figure 4D, F) and crystal violet staining (Figure 4G, I) to assess apoptosis and cell growth. Inhibiting the Aurora kinases together allowed NCI-H1693 cells to survive and grow whereas inhibiting Aurora A or B selectively was inhibitory. Consequently, selective concentrations of Aurora B, C inhibitors could convert the multiphasic “camelback” dose response pattern of Aurora A inhibitors into monophasic “resistant” dose response pattern when combined together in NCI-H1693 cells (Figure 4H, J).

Based on these observations, we hypothesized that pan-Aurora kinase inhibitors would be non- or minimally effective on NCI-H1693 cells when compared with the first response phases of MLN8237, VX-689, AZD1152 and GSK1070916. We performed biochemical assays identical to the ones performed with the four Aurora A or B and C selective inhibitors. We observed that pan-Aurora inhibitors, VX-680/Tozasertib (VX-680 henceforth) and PHA-739358/Danusertib (PHA-739358 henceforth) have a resistance response pattern resembling the second phase of multiphasic response of the first four selective inhibitors (Figure S1A-H).

To determine how frequently NSCLC cell lines survived simultaneous inhibition of all Aurora kinases, we measured the dose-responses to MLN8237 in a panel of 77 NSCLC and 4 immortalized human bronchial epithelial cell (HBEC) lines. More than fifty percent of these cell lines had a multiphasic camel-back drug response pattern with more cancer persister cells at the pan-Aurora kinase inhibitory phase in comparison to the responses at lower Aurora A-selective doses (Figure 5A). In addition, the rest of tested NSCLC lines were either uniformly sensitive or uniformly resistant to the effective doses of MLN8237 with a sigmoidal or monophasic response, respectively (Figure 5A). An identical screen with VX-689 produced results similar to those obtained with the screen of MLN8237 (Figure 5B). In these studies, Erlotinib, an EGFR-targeted therapy agent and FDA-approved drug for NSCLCs, was used as control in parallel to MLN8237 and VX-689, on the same day at identical conditions and no multiphasic “camelback” response pattern was observed (Figure 5C). Overall, our data indicated that the multiphasic response pattern against Aurora A inhibitors is common for NSCLC cell lines and more “persister” cells were generated when all Aurora kinases were inhibited in comparison to selective Aurora A inhibition.

To determine what type of growth cells adopt after the loss of Aurora kinase signaling, we examined cellular morphology and DNA content after inhibiting Aurora kinases individually or

in combination. After the inhibition of Aurora kinases with the non-selective high concentration of MLN8237, we observed that NCI-H1693 cells grow substantially in size instead of numbers and therefore, cellular ATP levels increase similar to untreated proliferating cells (Figure 6A-B). The average area of cells treated with pan-Aurora kinase inhibitor for four days increased and cells had much more nuclear DNA in comparison to the untreated ones (Figure 6C). Cell numbers were not increasing (Figure 6D) in the treated samples, but were balanced by increasing the cellular size. Therefore, total ATP levels present in the treated wells remained similar to the wells with untreated cells. DNA replication also continued (Figure 6D). Increasing DNA content and cell size are characteristics of an endocycle (Lee et al., 2009). Overall, our findings suggest that after inhibiting Aurora kinase signaling, cells omit all or most of mitosis, and continue with intact Gap (G) and Synthesis (S) phases of cell cycle (Figures 6E).

If an endocycle variant takes place and mitosis is avoided when Aurora kinase signaling is turned off, we hypothesized that mitotic machinery including spindle-related components and regulators should partially or completely be dispensable. Thus, cells would be non-responsive to anti-mitotic agents under these conditions instead of causing additive or synergistic effects whereas perturbing interphase cellular machineries should remain cytotoxic (Figure 7A). Thus, we tested NCI-H1693 cells with 17 anti-cancer or cytotoxic agents including 9 for interphase (Gemcitabine, Carboplatin, Cisplatin, Etoposide, Topotecan, Doxorubucin, Pemetrexed, Methotrexate, 5-Fluorouracil, Aphidicollin and Bafilomycin A) and 8 for mitosis (Paclitaxel, Docetaxel, Vinorelbine, Vinblastine, PLK1 inhibitor BI-6727 (Volasertib), CENPE inhibitor GSK923295, EG5 inhibitors Ispinesib and VS-83). For the cell viability assessments, the EC100 of each agent was used (Supplementary Table 1). Aurora kinase inhibition prevented toxicity from all anti-mitotic drugs whereas cells were sensitive to interphase perturbagens regardless of the presence of Aurora inhibitors (Figure 7B). In addition to individual treatments with these anti-cancer agents, we also added a cocktail of the eight anti-mitotic agents to our survey and observed that cancer persister cells generated by pan-Aurora kinase inhibition were able to avoid death even in that extreme condition (Figure 7B). In parallel to the cell viability assays, we stained NCI-H1693 cells with crystal violet to check the status of cell growth on day 7 in comparison to the cell density on Day 0. Our results confirmed that NCI-H1693 cells survived and continued to grow in the presence of all anti-mitotics and their cocktail, but not the anti-interphase perturbagens (Figure 7C). Lastly, we quantified the extent of tolerance of these anti-mitotic persister cells to individual anti-mitotic agents by performing cell viability assays with serial concentrations of eight anti-mitotic drugs in the presence and absence of pan-Aurora kinase inhibitors. We observed at least 4 logarithmic (log) magnitude of drug resistance to Paclitaxel, 5 logs to Docetaxel (Figure 7D), and at least 2 logs of significant resistance to others (Figure S2A-F).

Finally, we investigated whether the NCI-H1693 cells that had switched to endocycle could reenter the proliferative cell cycle. Four days after inhibiting Aurora kinase signaling with combinations of Aurora A inhibitor, MLN8237 and Aurora B, C inhibitors AZD1152 or GSK1070916 at concentrations selective for their primary targets, the media with the combination treatments was washed out and NCI-H1693 cells were allowed to grow in the absence of any drug treatments for 14 days. NCI-H1693 cells recovered from the combination treatment and were able to form colonies, indicating the ability of cells to

reenter the mitotic cell cycle (Figure 7E). In comparison, NCI-H1693 cells treated with Paclitaxel had significantly fewer colonies. These observations indicate that loss of Aurora kinase signaling initiates an endocycle, which maintains cell growth in size instead of numbers. These cells can re-enter a proliferative cell cycle when Aurora kinase signaling is restored (Figure 7F).

Discussion

Our results indicate that Aurora kinases function together to keep the cell in a proliferative cell cycle. In many cell types, only Aurora A and B kinases are expressed and the extent to which Aurora C plays a role in this activity is not determined by our work. In a majority of NSCLC cell lines, chemical inhibition of all family members of Aurora kinases allows the cells to adopt an alternative cell cycle where cells continue to replicate DNA and grow in size, but do not divide. In this state, cells are resistant to all anti-mitotic drugs tested because the mitotic machinery is no longer engaged. Our findings together suggest that Aurora kinases may operate as a cell cycle switch and their off status generates cancer cells tolerant to anti-mitotic therapy in those cell lines where the alternative cell cycle is available.

In the nature, there are numerous examples of alternative cell cycles, called endocycles (also known as endoreplication, endoreduplication or endomitosis), that generate healthy polyploid cells for specialized functions. Endocycling is essential for the proper development of specialized cell types in mammalian systems like megakaryocytes, placental trophoblast cells, hepatocytes and cardiomyocytes (Edgar et al., 2014). The level of ploidy varies dramatically among tissues, organs and species. Mammalian placental trophoblast cells can exhibit ploidy levels of 4096 times the haploid number of chromosomes (4096C) (Zybina, 1983; Zybina and Chernogriadakaia, 1976). Megakaryocytes generate nuclei with DNA content up to 128C (Ravid et al., 2002). The highest recorded level for hepatocytes and cardiomyocytes is 32C. By adulthood and with ageing, up to 70% of human and 85% of rodent cardiac myocytes are polyploid (Mollova et al., 2013; Soonpaa et al., 1996). The highest polyploidy level recorded in any animal is ~500,000C, reported from the silk-producing glands of silk moth *Bombyx mori* (Perdrix-Gillot, 1979). The neurons of mollusks exhibit remarkable variations of ploidy, ranging from a low 32C in the land snail *Triodopsis divesta* to an astonishing 200,000C in the giant neurons of the sea hare *Aplysia californica* (Lasek and Dower, 1971; Mandrioli et al., 2010). A range of 4C to 64C is typical in plants although the highest level of polyploidy observed in plants is 24,576C in the endosperm of *Arum maculatum* (Barow, 2006; Scholes and Paige, 2015).

Cancers can take advantage of polyploidy by creating heterogeneity of cell types, some of which are more drug resistant than the parental cells (Puig et al., 2008). It is possible that some cancer cells do this by adopting an alternate cell cycle program similar to those available to specialized cell types. In the brain, a blood-brain barrier is formed by endothelial cells and these specialized cell types are known to be decorated with efflux pumps and upregulate drug metabolizing enzymes (Arvanitis et al., 2019; Schinkel et al., 1994). The glial cells forming the barrier in fruit fly *Drosophila melanogaster* were shown to require polyploidization for proper differentiation (Unhavaithaya and Orr-Weaver, 2012; Von Stetina et al., 2018). In cancers, drug resistance mechanisms to lower the cytosolic drug concentrations with these two systems are well-documented and could originate from cancer cells that were capable of growing in endothelial cell-like endocycles.

Unexpected adverse interactions in clinical trials with combination therapies occur and mostly the reasons remain unknown. Currently, 60 clinical trials with MLN8237, 10 with VX-689, 12 with AZD1152, 14 with GSK1070916, 11 with VX-680 and 8 with PHA-739358 have been reported and among those many are performed in combination with other anti-mitotic drugs such as Taxanes and Vinca alkaloids. Among the concluded trials, some revealed that targeted mitotic inhibitors, including Aurora kinase inhibitors, were less effective than expected (Benada and Macurek, 2015; Manchado et al., 2012). Secondly, enlargement of cells in the non-responsive cancers or tumor models after treatments with various chemo- or -targeted therapies were previously reported (Puig et al., 2008). Moreover, increased cell size was also observed in studies with Aurora kinase-targeted therapies including MLN8237 (Haruki et al., 2017; Kogiso et al., 2018; Lee et al., 2019). However, thus far, no explanation of this unexpected effect has been provided. Our study presents a potential mechanistic explanation for these clinical results.

Lastly, the multiphasic dose-response pattern that we observed with inhibitors of Aurora kinase signaling is not appropriately recognized by the standard approaches for drug dose-response curve fitting. It was recently reported that the failure rate of the classical Hill equation is more than 25% in large scale screens (Di Veroli et al., 2015). In experiments investigating the response of NSCLC cell panels to synthetic chemicals (McMillan et al., 2018), we have observed that dose-responses poorly represented by sigmoidal curves are quite common. Some of these are undoubtably due to chemical solubility or other experimental artifacts, but our current report indicates that some indicate a biological response that is not considered by the assumptions underlying most commonly used curve fitting programs.

In summary, our data suggest that Aurora kinase signaling functions at the intersection between proliferative cell cycle and endocycle. Switching to endocycle variants creates growing cancer cells tolerant to anti-mitotic therapy. These cancer cells also retain the capability to reenter the proliferative cell cycle after the treatments are terminated.

Methods

Cell lines

NSCLC and immortalized HBEC lines were generated by the laboratories of John Minna and Adi Gazdar and their identities have been confirmed by short tandem repeat analysis of cellular DNA (Promega Corp, Madison, WI, USA). All cell lines were determined to be mycoplasma free by testing with the e-Myco Plus Mycoplasma PCR Detection Kit (Bulldog Bio, 2523448). NSCLC lines were cultured in RPMI-1640 medium (GIBCO, 11875) supplemented with 10% fetal bovine serum (v/v) (Atlanta Biological, S11550). HBEC lines were grown in Keratinocyte-SFM medium (GIBCO, 17005) supplemented with EGF and keratinocyte extract (provided by the manufacturer). HBEC3-KT, HBEC30-KT and HBEC34-KT are HBECs immortalized with stable expression of CDK4 and hTERT (Ramirez et al., 2004).

Reagents

MLN8237 (Alisertib) (ChemieTek, CT-M8237), VX-689 (Selleckchem, S2770), AZD1152 (Barasertib) (Selleckchem, S1147), GSK1070916 (Selleckchem, S2740), VX-680 (Tozasertib) (Chemietek, CT-VX680), PHA-739358 (Danusertib) (Selleckchem, S1107), Paclitaxel (LC Labs, P-9600), Docetaxel (Sigma-Aldrich, 01885), Vinorelbine detartrate salt hydrate (Sigma-Aldrich, V2264), Vinblastine sulfate (Sigma-Aldrich, V1377), BI 6727 (Volasertib) (Selleckchem, S2235), GSK923295 (Selleckchem, S7090), Ispinesib (Cayman Chemical Company, 18014), VS-83 (Calbiochem, 178273), Gemcitabine (ChemieTek, CT-GEM), Carboplatin (Sigma-Aldrich, C2538), Cisplatin (Sigma-Aldrich, 232120), Etoposide (LC Labs, E-4488), Topotecan (Tocris, 4562), Doxorubucin hydrochloride (Sigma-Aldrich, D1515), Pemetrexed (Tocris, 6185), Methotrexate (Tocris, 1230), 5-Fluorouracil (Sigma-Aldrich, F6627), Aphidicollin (Calbiochem, 178273), Bafilomycin A (Sigma-Aldrich, B1793), Erlotinib (LC Labs, E-4497) was purchased in powder form and stored at 10 mM or 20 mM stock concentrations in dimethyl sulfoxide (DMSO) at −20 °C. Phospho-AURKA (Thr288)/AURKB (Thr232)/AURKC (Thr198) (Cell Signaling, rabbit mAb, 2914, 1:1,000 dilution), Phospho-Histone H3 (Ser10) (Cell Signaling, rabbit mAb, 33770, 1:1,000 dilution) and β-Actin (MP Biomedicals, mouse mAb, 69100, 1:10,000 dilution) antibodies were used for immunoblotting assays. Texas Red™-X Phalloidin (ThermoFisher Scientific, T7471, 1:100 dilution) and Hoechst 33342 reagent (ThermoFisher Scientific, H3570, 1:2000 dilution) were used for immunofluorescence assays.

Microplate drug sensitivity assays

NCI-H1693 cells (3,000 per well) were seeded in 96-well plates and incubated at 37 °C for 24 h. Treatment with vehicle (DMSO) or serial dilutions of the indicated compounds in 9 concentrations from 1 to 33,300 nM were performed in triplicate (final DMSO concentration=0.34% in all wells). After 96 h, media were removed and cell viability was measured with a CellTiter-Glo assay (Promega, G7573).

A dose–response study of a panel of NSCLC and HBEC cell lines with MLN8237 (Alisertib), VX-689 and Erlotinib was performed in 384-well plate format. Cells were dispensed at a density of 1,000–1,500 cells per well with an automated liquid dispenser (BioTek MicroFlo; Thermo-Fisher, Inc.). Each concentration was screened in triplicate. Cells were incubated for 24 h at 37 °C in the presence of 5% CO_2.with an automated liquid dispenser (BioTek MicroFlo; Thermo-Fisher, Inc.) Drugs/chemicals were dosed in DMSO at 12 concentrations ranging from 50 pM to 50 μM (half-log dilutions) in triplicate, using an Echo 555 acoustical transfer instrument. After incubating the cells at 37 °C for 96 h, cell viability was measured with a CellTiter-Glo assay. The comparative tests of three agents were performed on the same days, in identical conditions. Dose responses of each cell line to each agent were assessed at the indicated concentrations individually. Concentrations that caused increase in the measured viability after the initial cytotoxic effect of respective agent were colored in red.

Microplate apoptosis assay

Treatments of the indicated compounds were performed in the same manner with the microplate drug sensitivity assays in 96-well plate format. 48 hours after treatments, culture media were removed by centrifuging the assay plates upside down in liquid-collecting containers at 30*g* for 1 min. Caspase 3 and/or 7 activity was assessed with Caspase-Glo 3/7 assay purchased from Promega (G8090).

Crystal violet staining assay

NCI-H1693 cells (1 × 10^5 per well) were seeded in 6-well plates and incubated at 37 °C for 24 h. Treatment with vehicle (DMSO) or serial dilutions of the indicated compounds in 10 indicated concentrations were performed (final DMSO concentration=0.34% in all wells). After seven days, media were removed and cell growth was assessed with a crystal violet staining assay solution (6% glutaraldehyde, 0.5% crystal violet (w/v) in water).

Western blotting

In all, 2 × 10^5 cells were treated with the indicated compounds at indicated concentrations in six-well format. Forty-eight hours after treatments, the culture medium was aspirated and cells were washed with PBS. Cells were lysed in RIPA lysis buffer (50 mM Tris buffer pH 8, 150 mM NaCl, 1% NP-40, 0.5% sodium, 0.1% SDS, 0.5% Sodium deoxycholate) supplemented with protease and phosphatase inhibitors. The protein concentrations of cell lysates were measured with the Protein DC assay (Bio-Rad, 500-0111). Phosphorylation of histone H3 and Aurora kinases A, B, C, and β-Actin expression as internal control were monitored by immunoblotting with monoclonal antibodies.

Light microscope and immunofluorescence assay

Cells in transparent bottom plates were fixed with 4% formaldehyde in PBS for 15 min at room temperature. After washing with PBS, cells were permeabilized with 0.25% Triton-X in PBS for 15 min at room temperature. After washing with PBS, cells were incubated with 10% Bovine Serum Albumin (BSA) blocking solution for 1 h. Next, cells were immunostained with Texas Red™-X Phalloidin and/or Hoechst 33342 reagent for 1 h. Microscopic observations were performed on an EVOS FL Cell Imaging System. Mean nuclear area of cells after the treatments with the indicated compounds were calculated with the ImageJ software and graphed.

Acknowledgements

We thank Bruce Posner and the personnel of the Simmons Comprehensive Cancer Center High-throughput Screening Core Facility for aid in dose-response experiments on the NSCLC cell line panel. The human tumor-derived cell panel was created by Drs. John D. Minna and Adi F. Gazdar. This work was supported by grants CA176284 and CA221978 to MGR.

Author Contributions

V.T. designed and performed the experiments. V.T. and M.G.R. conceived the study, analyzed data and wrote the manuscript.

Declaration of Interests

The authors declare no competing financial interests.

References

Anderson, K., Lai, Z., McDonald, O.B., Stuart, J.D., Nartey, E.N., Hardwicke, M.A., Newlander, K., Dhanak, D., Adams, J., Patrick, D.*, et al.* (2009). Biochemical characterization of GSK1070916, a potent and selective inhibitor of Aurora B and Aurora C kinases with an extremely long residence time1. Biochem J *420*, 259-265.

Arvanitis, C.D., Ferraro, G.B., and Jain, R.K. (2019). The blood-brain barrier and blood-tumour barrier in brain tumours and metastases. Nat Rev Cancer.
Bain, J., McLauchlan, H., Elliott, M., and Cohen, P. (2003). The specificities of protein kinase inhibitors: an update. Biochem J *371*, 199-204.
Bain, J., Plater, L., Elliott, M., Shpiro, N., Hastie, C.J., McLauchlan, H., Klevernic, I., Arthur, J.S., Alessi, D.R., and Cohen, P. (2007). The selectivity of protein kinase inhibitors: a further update. Biochem J *408*, 297-315.
Barow, M. (2006). Endopolyploidy in seed plants. Bioessays *28*, 271-281.
Benada, J., and Macurek, L. (2015). Targeting the Checkpoint to Kill Cancer Cells. Biomolecules *5*, 1912-1937.
Bolton, M.A., Lan, W., Powers, S.E., McCleland, M.L., Kuang, J., and Stukenberg, P.T. (2002). Aurora B kinase exists in a complex with survivin and INCENP and its kinase activity is stimulated by survivin binding and phosphorylation. Molecular biology of the cell *13*, 3064-3077.
Bury, L., Coelho, P.A., Simeone, A., Ferries, S., Eyers, C.E., Eyers, P.A., Zernicka-Goetz, M., and Glover, D.M. (2017). Plk4 and Aurora A cooperate in the initiation of acentriolar spindle assembly in mammalian oocytes. The Journal of cell biology *216*, 3571-3590.
Cervantes, A., Elez, E., Roda, D., Ecsedy, J., Macarulla, T., Venkatakrishnan, K., Roselló, S., Andreu, J., Jung, J., Sanchis-Garcia, J.M.*, et al.* (2012). Phase I pharmacokinetic/pharmacodynamic study of MLN8237, an investigational, oral, selective aurora a kinase inhibitor, in patients with advanced solid tumors. Clin Cancer Res *18*, 4764-4774.
Crosio, C., Fimia, G.M., Loury, R., Kimura, M., Okano, Y., Zhou, H., Sen, S., Allis, C.D., and Sassone-Corsi, P. (2002). Mitotic phosphorylation of histone H3: spatio-temporal regulation by mammalian Aurora kinases. Molecular and cellular biology *22*, 874-885.
Davies, S.P., Reddy, H., Caivano, M., and Cohen, P. (2000). Specificity and mechanism of action of some commonly used protein kinase inhibitors. Biochem J *351*, 95-105.
Di Veroli, G.Y., Fornari, C., Goldlust, I., Mills, G., Koh, S.B., Bramhall, J.L., Richards, F.M., and Jodrell, D.I. (2015). An automated fitting procedure and software for dose-response curves with multiphasic features. Sci Rep *5*, 14701.
Edgar, B.A., Zielke, N., and Gutierrez, C. (2014). Endocycles: a recurrent evolutionary innovation for post-mitotic cell growth. Nat Rev Mol Cell Biol *15*, 197-210.
Giet, R., and Glover, D.M. (2001). Drosophila aurora B kinase is required for histone H3 phosphorylation and condensin recruitment during chromosome condensation and to organize the central spindle during cytokinesis. The Journal of cell biology *152*, 669-682.
Gopalan, G., Chan, C.S., and Donovan, P.J. (1997). A novel mammalian, mitotic spindle-associated kinase is related to yeast and fly chromosome segregation regulators. The Journal of cell biology *138*, 643-656.
Gupta, S. (2000). Hepatic polyploidy and liver growth control. Semin Cancer Biol *10*, 161-171.
Hanahan, D., and Weinberg, R.A. (2011). Hallmarks of cancer: the next generation. Cell *144*, 646-674.
Hangauer, M.J., Viswanathan, V.S., Ryan, M.J., Bole, D., Eaton, J.K., Matov, A., Galeas, J., Dhruv, H.D., Berens, M.E., Schreiber, S.L.*, et al.* (2017). Drug-tolerant persister cancer cells are vulnerable to GPX4 inhibition. Nature *551*, 247-250.
Hannak, E., Kirkham, M., Hyman, A.A., and Oegema, K. (2001). Aurora-A kinase is required for centrosome maturation in Caenorhabditis elegans. The Journal of cell biology *155*, 1109-1116.
Haruki, T., Papari-Zareei, M., Zhang, W., Zhang, Y., Stastny, V., Minna, J., and Gazdar, A. (2017). Relationship Between MYC Family Status and Sensitivity to Aurora Kinase Inhibitors in Neuroendocrine and Other Lung Cancer Cell Lines. J Thorac Oncol *12*, S2044-S2044.
Janne, P.A. (2008). Challenges of detecting EGFR T790M in gefitinib/erlotinib-resistant tumours. Lung Cancer *60 Suppl 2*, S3-9.

Kogiso, M., Qi, L., Braun, F.K., Injac, S.G., Zhang, L., Du, Y., Zhang, H., Lin, F.Y., Zhao, S., Lindsay, H.*, et al.* (2018). Concurrent Inhibition of Neurosphere and Monolayer Cells of Pediatric Glioblastoma by Aurora A Inhibitor MLN8237 Predicted Survival Extension in PDOX Models. Clin Cancer Res *24*, 2159-2170.

Lasek, R.J., and Dower, W.J. (1971). Aplysia californica: analysis of nuclear DNA in individual nuclei of giant neurons. Science *172*, 278-280.

Lee, H.O., Davidson, J.M., and Duronio, R.J. (2009). Endoreplication: polyploidy with purpose. Genes Dev *23*, 2461-2477.

Lee, J.W., Parameswaran, J., Sandoval-Schaefer, T., Eoh, K.J., Yang, D.H., Zhu, F., Mehra, R., Sharma, R., Gaffney, S.G., Perry, E.B.*, et al.* (2019). Combined Aurora Kinase A (AURKA) and WEE1 Inhibition Demonstrates Synergistic Antitumor Effect in Squamous Cell Carcinoma of the Head and Neck. Clin Cancer Res *25*, 3430-3442.

MacAuley, A., Cross, J.C., and Werb, Z. (1998). Reprogramming the cell cycle for endoreduplication in rodent trophoblast cells. Molecular biology of the cell *9*, 795-807.

Manchado, E., Guillamot, M., and Malumbres, M. (2012). Killing cells by targeting mitosis. Cell Death Differ *19*, 369-377.

Mandrioli, M., Mola, L., Cuoghi, B., and Sonetti, D. (2010). Endoreplication: a molecular trick during animal neuron evolution. Q Rev Biol *85*, 159-169.

McMillan, E.A., Ryu, M.J., Diep, C.H., Mendiratta, S., Clemenceau, J.R., Vaden, R.M., Kim, J.H., Motoyaji, T., Covington, K.R., Peyton, M.*, et al.* (2018). Chemistry-First Approach for Nomination of Personalized Treatment in Lung Cancer. Cell *173*, 864-878 e829.

Mollova, M., Bersell, K., Walsh, S., Savla, J., Das, L.T., Park, S.Y., Silberstein, L.E., Dos Remedios, C.G., Graham, D., Colan, S.*, et al.* (2013). Cardiomyocyte proliferation contributes to heart growth in young humans. Proc Natl Acad Sci U S A *110*, 1446-1451.

Mortlock, A.A., Foote, K.M., Heron, N.M., Jung, F.H., Pasquet, G., Lohmann, J.J., Warin, N., Renaud, F., De Savi, C., Roberts, N.J.*, et al.* (2007). Discovery, synthesis, and in vivo activity of a new class of pyrazoloquinazolines as selective inhibitors of aurora B kinase. Journal of medicinal chemistry *50*, 2213-2224.

Otto, T., and Sicinski, P. (2017). Cell cycle proteins as promising targets in cancer therapy. Nat Rev Cancer *17*, 93-115.

Pao, W., Miller, V.A., Politi, K.A., Riely, G.J., Somwar, R., Zakowski, M.F., Kris, M.G., and Varmus, H. (2005). Acquired resistance of lung adenocarcinomas to gefitinib or erlotinib is associated with a second mutation in the EGFR kinase domain. PLoS Med *2*, e73.

Perdrix-Gillot, S. (1979). DNA synthesis and endomitoses in the giant nuclei of the silkgland of Bombyx mori. Biochimie *61*, 171-204.

Puig, P.E., Guilly, M.N., Bouchot, A., Droin, N., Cathelin, D., Bouyer, F., Favier, L., Ghiringhelli, F., Kroemer, G., Solary, E.*, et al.* (2008). Tumor cells can escape DNA-damaging cisplatin through DNA endoreduplication and reversible polyploidy. Cell Biol Int *32*, 1031-1043.

Ramirez, R.D., Sheridan, S., Girard, L., Sato, M., Kim, Y., Pollack, J., Peyton, M., Zou, Y., Kurie, J.M., Dimaio, J.M.*, et al.* (2004). Immortalization of human bronchial epithelial cells in the absence of viral oncoproteins. Cancer Res *64*, 9027-9034.

Ravid, K., Lu, J., Zimmet, J.M., and Jones, M.R. (2002). Roads to polyploidy: the megakaryocyte example. J Cell Physiol *190*, 7-20.

Schinkel, A.H., Smit, J.J., van Tellingen, O., Beijnen, J.H., Wagenaar, E., van Deemter, L., Mol, C.A., van der Valk, M.A., Robanus-Maandag, E.C., te Riele, H.P.*, et al.* (1994). Disruption of the mouse mdr1a P-glycoprotein gene leads to a deficiency in the blood-brain barrier and to increased sensitivity to drugs. Cell *77*, 491-502.

Scholes, D.R., and Paige, K.N. (2015). Plasticity in ploidy: a generalized response to stress. Trends Plant Sci *20*, 165-175.

Simpson, A.J., Caballero, O.L., Jungbluth, A., Chen, Y.T., and Old, L.J. (2005). Cancer/testis antigens, gametogenesis and cancer. Nat Rev Cancer *5*, 615-625.

Sinha, D., Duijf, P.H.G., and Khanna, K.K. (2019). Mitotic slippage: an old tale with a new twist. Cell cycle *18*, 7-15.
Soonpaa, M.H., Kim, K.K., Pajak, L., Franklin, M., and Field, L.J. (1996). Cardiomyocyte DNA synthesis and binucleation during murine development. Am J Physiol *271*, H2183-2189.
Steinmetz, M.O., and Prota, A.E. (2018). Microtubule-Targeting Agents: Strategies To Hijack the Cytoskeleton. Trends Cell Biol *28*, 776-792.
Tagal, V., Wei, S., Zhang, W., Brekken, R.A., Posner, B.A., Peyton, M., Girard, L., Hwang, T., Wheeler, D.A., Minna, J.D.*, et al.* (2017). SMARCA4-inactivating mutations increase sensitivity to Aurora kinase A inhibitor VX-680 in non-small cell lung cancers. Nature communications *8*, 14098.
Unhavaithaya, Y., and Orr-Weaver, T.L. (2012). Polyploidization of glia in neural development links tissue growth to blood-brain barrier integrity. Genes Dev *26*, 31-36.
Viswanathan, V.S., Ryan, M.J., Dhruv, H.D., Gill, S., Eichhoff, O.M., Seashore-Ludlow, B., Kaffenberger, S.D., Eaton, J.K., Shimada, K., Aguirre, A.J.*, et al.* (2017). Dependency of a therapy-resistant state of cancer cells on a lipid peroxidase pathway. Nature *547*, 453-457.
Von Stetina, J.R., Frawley, L.E., Unhavaithaya, Y., and Orr-Weaver, T.L. (2018). Variant cell cycles regulated by Notch signaling control cell size and ensure a functional blood-brain barrier. Development *145*.
Walter, A.O., Seghezzi, W., Korver, W., Sheung, J., and Lees, E. (2000). The mitotic serine/threonine kinase Aurora2/AIK is regulated by phosphorylation and degradation. Oncogene *19*, 4906-4916.
Zhang, W., Girard, L., Zhang, Y.A., Haruki, T., Papari-Zareei, M., Stastny, V., Ghayee, H.K., Pacak, K., Oliver, T.G., Minna, J.D.*, et al.* (2018). Small cell lung cancer tumors and preclinical models display heterogeneity of neuroendocrine phenotypes. Transl Lung Cancer Res *7*, 32-49.
Zybina, E.V. (1983). [Different modes of cell reproduction in the placental differentiation of mammals]. Tsitologiia *25*, 1103-1119.
Zybina, E.V., and Chernogriadakaia, N.A. (1976). [A study of the polyploid nuclei of the giant trophoblast cells of several species of rodents using phase contrast microscopy]. Tsitologiia *18*, 161-165.

Main Figure Titles and Legends

Figure 1. There are distinctly different response phenotypes to Aurora Kinase inhibition. (A-F) Cells were treated with Aurora A selective inhibitors MLN8237 or VX-689 at the concentrations shown and cell viability was measured with a CellTiter-Glo assay, which measures cellular ATP as an indicator of living cells. Data are means of triplicate biological replicates and error bars are standard deviations (s.d). Some error bars are smaller than the data symbols. Cell lines representative of three distinct dose response curves are shown.

Figure 2. Aurora A inhibitors at higher concentrations antagonize their own cytotoxic activity and restore growth. (A) NCI-H1693 cells were treated with serial concentrations of MLN8237 for four days and cell viability was measured with a CellTiter-Glo assay, which measures ATP. (B) NCI-H1693 cell line was treated with serial concentrations of MLN8237 for two days and active apoptosis was measured with a CaspaseGlo 3/7 assay. (C, D) CellTiter-Glo and CaspaseGlo 3/7 assays were repeated with VX-689 treatments. Data are means of triplicate biological replicates with s.d. Some error bars are smaller than the data symbols. (E) NCI-H1693 cells were treated with serial concentrations of MLN8237 or (G) VX-689 for seven days and cell growth quantified with a crystal violet staining assay. (F) Cell lysates of NCI-H1693 cell line were collected 48-hours after treating with MLN8237 or (H) VX-689 and immunoblotted to measure phosphorylated histone H3 and phosphorylated Aurora A, B, and C. Paclitaxel was used in both sets of immunoblots as positive control and B-Actin was used as internal immunoblotting control. (I, J) Overlay of cell viability, caspase 3/7 activity and crystal violet staining images with immunoblotting results at Aurora A kinase selective and non-selective (pan-Aurora kinase) inhibitory concentrations of MLN8237 and VX-689.

Figure 3. Aurora B, C inhibitors exhibit a camelback drug response pattern similar to Aurora A inhibitors. (A) Cell lysates of NCI-H1693 cells were collected 48-hours after treating with AZD1152 (Barasertib) or (B) GSK1070916 and immunoblotted to monitor phosphorylated histone H3 and phosphorylated Aurora A, B, C levels. Paclitaxel was used in both sets of immunoblots as positive control and B-Actin was used as internal immunoblotting control. (C) NCI-H1693 cells were treated with serial concentrations of AZD1152 for four days and cell viability was measured with a CellTiter-Glo assay. (D) NCI-H1693 cells were treated with serial concentrations of AZD1152 for two days and cell death was measured with a CaspaseGlo 3/7 assay. (E, F) Assays were repeated with GSK1070916 treatments. Data are means of triplicate biological replicates with s.d. Some error bars are smaller than the data symbols. (G) NCI-H1693 cell line was treated with serial concentrations of AZD1152 or (H) GSK1070916 for seven days and cell growth was measured with a crystal violet staining assay. (I-J) Overlay of cell viability, caspase 3/7 activity and crystal violet staining images with immunoblotting results at selective and non-selective concentrations of AZD1152 and GSK1070916.

Figure 4. Combining Aurora A and B, C inhibitors at concentrations selective for their primary targets prevents cytotoxicity and allows cell growth. (A) Cell lysates of NCI-H1693 cells were collected 48-hours after treating with combinations of MLN8237 and AZD1152 or (B) MLN8237 and GSK1070916 and immunoblotted to detect phosphorylated histone H3 and phosphorylated Aurora A, B, C. Paclitaxel was used in both sets of immunoblots as a positive control and β-Actin was used as an internal immunoblotting

control. (C) NCI-H1693 cells were treated with combinations of MLN8237 and AZD1152 at concentrations selective for their primary targets for four days and cell viability was measured with a CellTiter-Glo assay. (D) NCI-H1693 cells were treated with combinations of MLN8237 and AZD1152 at their selective for two days and cell death was measured with a CaspaseGlo 3/7 assay. (E, F) Identical assays were repeated with GSK1070916 treatments. (G) NCI-H1693 cells were treated with combinations of Aurora A and B/C selective inhibitors for seven days and cell growth was measured with a crystal violet staining assay. (H) NCI-H1693 cells were treated with serial concentrations of MLN8237 in combination with serial dilutions of AZD1152 for four days and cell viability was measured with a CellTiter-Glo assay. (I-J) Identical assays were repeated with GSK1070916 treatments. Data from CellTiter-Glo and CaspaseGlo 3/7 assays are presented as means of triplicate biological replicates with s.d. Some error bars are smaller than the data symbols.

Figure 5. Survey of a NSCLC line panel reveals that more than 50% of cell lines have more cancer persister cells at higher concentrations of Aurora kinase A inhibitors. (A) A panel of NSCLC and HBEC lines was treated with MLN8237, (B) VX-689 or (C) Erlotinib. The results of dose–response experiments are shown in heatmap format. Decrease in viability in comparison to the untreated control is shown in shades of gray and white. Increase in viability in comparison to the cytotoxicity induced at lower concentrations is colored in shades of red.

Figure 6. Loss of Aurora kinase signaling allows cells to adopt a cell cycle variant, which produces enlarged cells with high DNA content. (A) NCI-H1693 cells were treated with 0.41 μM of MLN8237 for four days and the ATP present was measured with a CellTiter-Glo assay. (B) NCI-H1693 cells were treated with 0.41 μM of MLN8237 for 20 days, stained with Phalloidin (red) and Hoechst (blue), and visualized at 10X magnification (Scale bar, 400 μM). (C) NCI-H1693 cells were treated with 0.41 μM of MLN8237 for four days and visualized with bright-field or fluorescent microscopy at 10X magnification. Hoechst reagent was used to visualize the nuclei (Scale bar, 400 μM). (D) The numbers of cells and their mean nuclear area from treated and untreated control samples are graphed. (E) A proposed model of an endocycle induced with the loss of Aurora kinase signaling.

Figure 7. Inhibition of Aurora kinase signaling provides resistance to anti-mitotic toxins, but not interphase toxins. (A) NCI-H1693 cells were co-treated with DMSO or 0.5 μM of MLN8237 and IC100 concentrations of interphase or mitotic perturbagens. (B) Cell viability and growth were assessed with a CellTiter-Glo assay (after four days of treatment) or (C) crystal violet staining assay (after seven days of treatment), respectively. (D) NCI-H1693 cells were co-treated with DMSO or 0.5 μM of MLN8237 and serial concentrations of Paclitaxel or Docetaxel. Cell viability was measured with a CellTiter-Glo assay. (E) NCI-H1693 cell line was treated with 0.1 μM of MLN8237 and 0.2 μM AZD1152 or 20 nM GSK1070916 for four days. Treatment media were replaced with drug-free media for 14 days. Colony formation was measured with a crystal violet staining assay. Data of CellTiter-Glo assay are means of triplicate biological replicates with s.d. Some error bars are smaller than the data symbols. (F) Proposed model of the cellular life cycle in the absence of Aurora kinase signaling.

Supplemental Figure Titles and Legends

Figure S1. Pan-Aurora kinase inhibitors do not inhibit growth of NCI-H1693 cells. (A) Cell lysates of NCI-H1693 cells were collected 48-hours after treating with VX-680 or (B) PHA-739358 (Danusertib) and immunoblotted to detect phosphorylated histone H3 and phosphorylated Aurora A, B, C. Paclitaxel was used in both sets of immunoblots as a positive control and B-Actin was used as an internal immunoblotting control. (C) NCI-H1693 cells were treated with serial concentrations of VX-680 for four days and cell viability was measured with a CellTiter-Glo assay. (D) NCI-H1693 cells were treated with serial concentrations of VX-680 for two days and apoptosis was measured with a CaspaseGlo 3/7 assay. (E, F) Assays were repeated with PHA-739358 treatments. Data are means of triplicate biological replicates with s.d. Some error bars are smaller than the data symbols. (G) NCI-H1693 cell line was treated with serial concentrations of VX-680 or (H) PHA-739358 for seven days and cell growth was measured with a crystal violet staining assay. A concentration of MLN8237 specific for Aurora kinase A and an EC100 concentration of Paclitaxel were used as controls. (I-J) Overlay of cell viability, caspase 3/7 activity and crystal violet staining images with immunoblotting results.

Figure S2. Endocycling cells resist anti-mitotic perturbagens. (A) Vinorelbine, (B) Vinblastine, (C) GSK923295, (D) BI 6727 (Volasertib), (E) Ispinesib or (F) VS-83 for four days and cell viability was measured with a CellTiter-Glo assay. Data are means of triplicate biological replicates with s.d. Some error bars are smaller than the data symbols.

Supplemental Table 1. EC100 values of all used FDA-approved chemotherapy agents for NSCLCs or cytotoxic poisons in NCI-H1693

Drug	EC100 (μM)
Paclitaxel	**0.02**
Docetaxel	**0.02**
Vinorelbine	**0.02**
Vinblastine	**0.02**
BI 6727 (Volasertib)	**0.1**
GSK923295	**0.1**
Ispinesib	**0.02**
VS-83	**10**
Gemcitabine	**0.1**
Topotecan-HCl	**0.2**

Methotrexate	**0.2**
Pemetrexed	**1**
Cisplatin	**20**
Carboplatin	**100**
Doxorubucin	**2**
Aphidicollin	**5**
Bafilomycin A	**0.02**
5-Fluorouracil	**20**

1

Figure 1

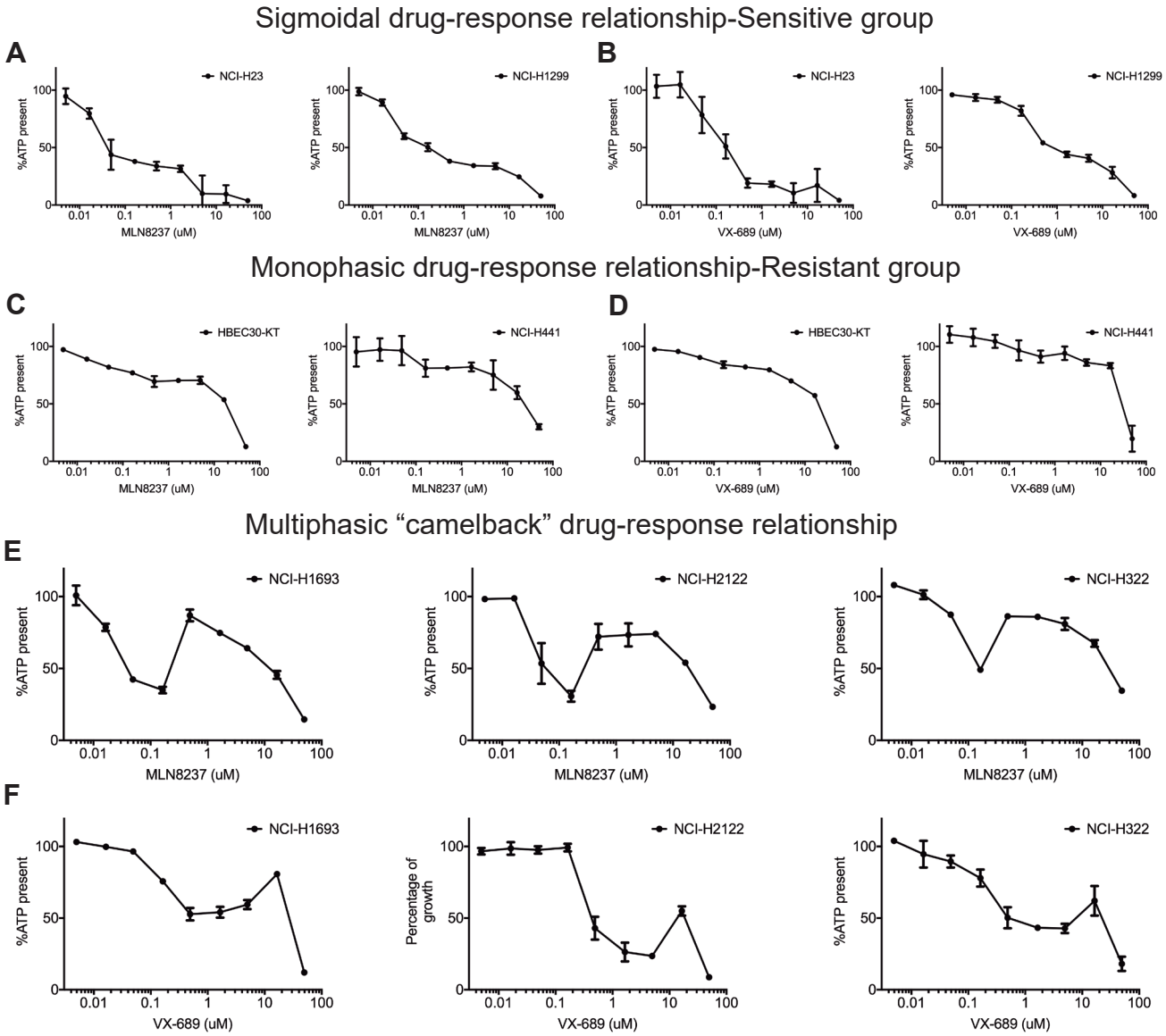
Sigmoidal drug-response relationship-Sensitive group
A
B
NCI-H23
NCI-H1299
%ATP present
MLN8237 (uM)
VX-689 (uM)
Monophasic drug-response relationship-Resistant group
C
D
HBEC30-KT
NCI-H441
Multiphasic "camelback" drug-response relationship
E
F
NCI-H1693
NCI-H2122
NCI-H322
Percentage of growth

Figure 2

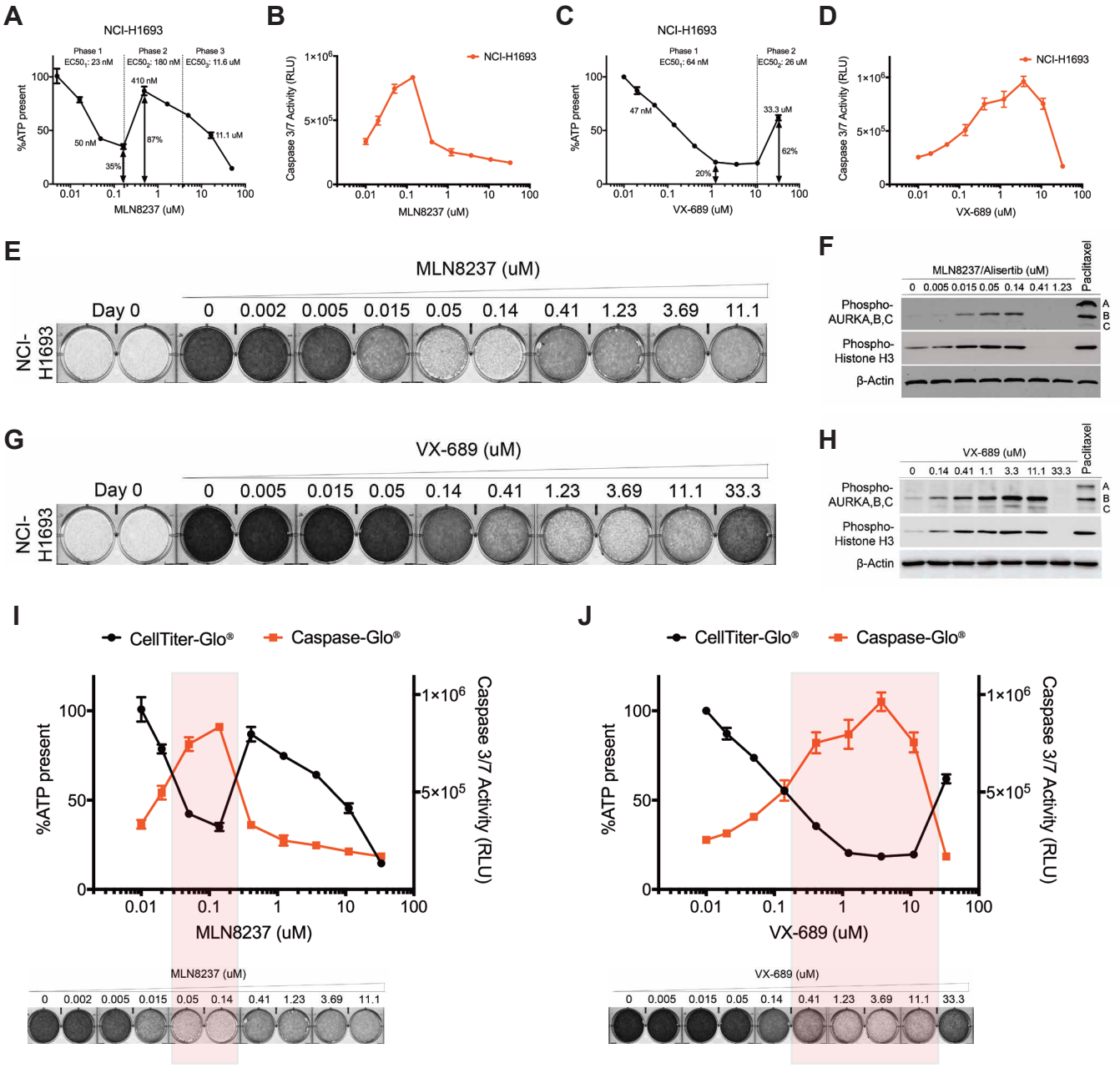
A
NCI-H1693
Phase 1
EC50$_1$: 23 nM
Phase 2
EC50$_2$: 180 nM
Phase 3
EC50$_3$: 11.6 uM
410 nM
50 nM
87%
35%
11.1 uM
%ATP present
MLN8237 (uM)
B
NCI-H1693
Caspase 3/7 Activity (RLU)
MLN8237 (uM)
C
NCI-H1693
Phase 1
EC50$_1$: 64 nM
Phase 2
EC50$_2$: 26 uM
47 nM
33.3 uM
62%
20%
%ATP present
VX-689 (uM)
D
NCI-H1693
Caspase 3/7 Activity (RLU)
VX-689 (uM)
E
MLN8237 (uM)
Day 0
0 0.002 0.005 0.015 0.05 0.14 0.41 1.23 3.69 11.1
NCI-H1693
F
MLN8237/Alisertib (uM)
0 0.005 0.015 0.05 0.14 0.41 1.23
Paclitaxel
Phospho-AURKA,B,C
A
B
C
Phospho-Histone H3
β-Actin
G
VX-689 (uM)
Day 0
0 0.005 0.015 0.05 0.14 0.41 1.23 3.69 11.1 33.3
NCI-H1693
H
VX-689 (uM)
0 0.14 0.41 1.1 3.3 11.1 33.3
Paclitaxel
Phospho-AURKA,B,C
A
B
C
Phospho-Histone H3
β-Actin
I
CellTiter-Glo®
Caspase-Glo®
%ATP present
Caspase 3/7 Activity (RLU)
MLN8237 (uM)
MLN8237 (uM)
0 0.002 0.005 0.015 0.05 0.14 0.41 1.23 3.69 11.1
J
CellTiter-Glo®
Caspase-Glo®
%ATP present
Caspase 3/7 Activity (RLU)
VX-689 (uM)
VX-689 (uM)
0 0.005 0.015 0.05 0.14 0.41 1.23 3.69 11.1 33.3

Figure 3

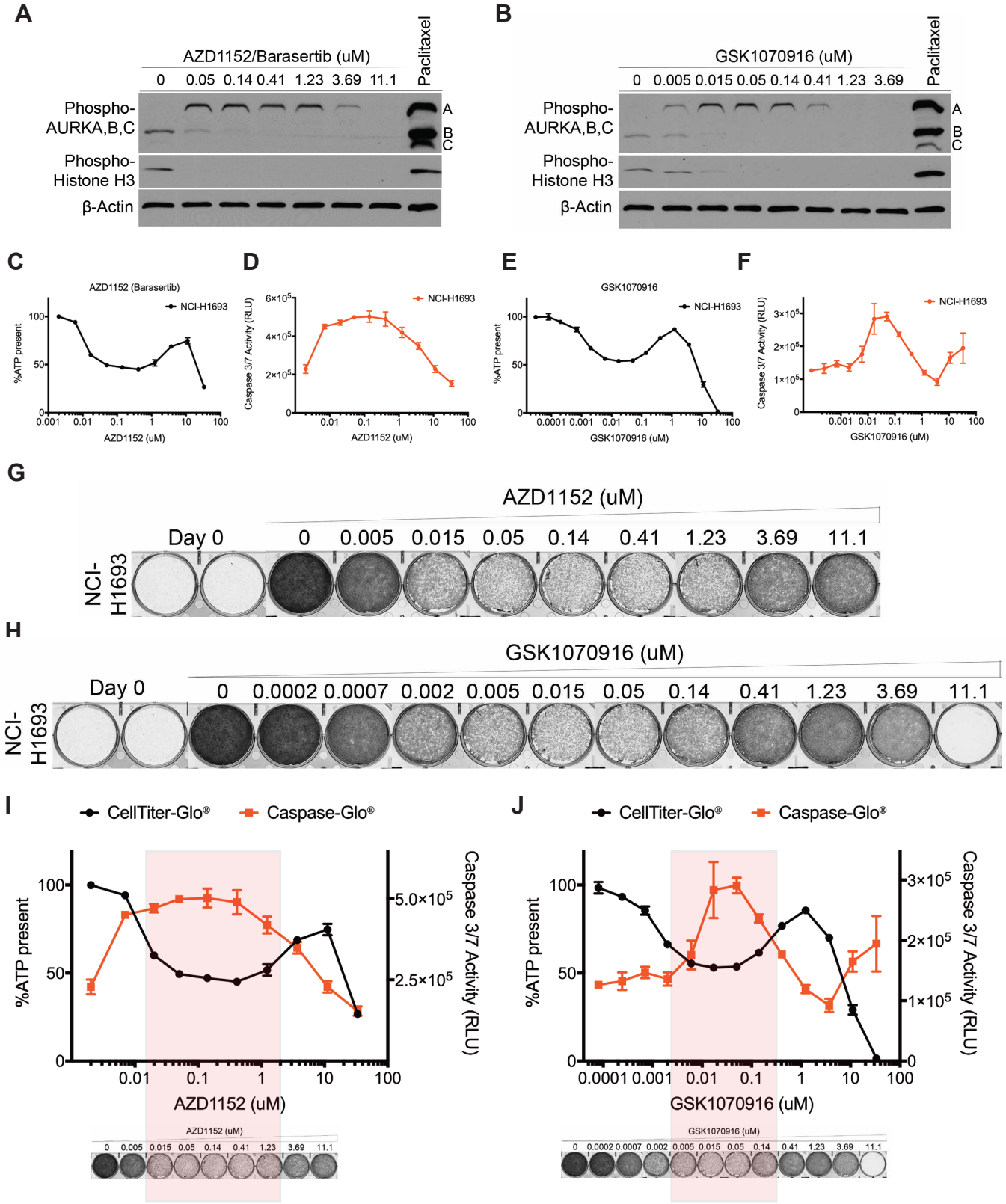
A
AZD1152/Barasertib (uM)
0 0.05 0.14 0.41 1.23 3.69 11.1
Paclitaxel
Phospho-AURKA,B,C
Phospho-Histone H3
β-Actin
A
B
C
B
GSK1070916 (uM)
0 0.005 0.015 0.05 0.14 0.41 1.23 3.69
Paclitaxel
Phospho-AURKA,B,C
Phospho-Histone H3
β-Actin
C
AZD1152 (Barasertib)
NCI-H1693
%ATP present
AZD1152 (uM)
D
NCI-H1693
Caspase 3/7 Activity (RLU)
AZD1152 (uM)
E
GSK1070916
NCI-H1693
%ATP present
GSK1070916 (uM)
F
NCI-H1693
Caspase 3/7 Activity (RLU)
GSK1070916 (uM)
G
AZD1152 (uM)
Day 0
0 0.005 0.015 0.05 0.14 0.41 1.23 3.69 11.1
NCI-H1693
H
GSK1070916 (uM)
Day 0
0 0.0002 0.0007 0.002 0.005 0.015 0.05 0.14 0.41 1.23 3.69 11.1
NCI-H1693
I
CellTiter-Glo®
Caspase-Glo®
%ATP present
Caspase 3/7 Activity (RLU)
AZD1152 (uM)
J
CellTiter-Glo®
Caspase-Glo®
%ATP present
Caspase 3/7 Activity (RLU)
GSK1070916 (uM)

Figure 4

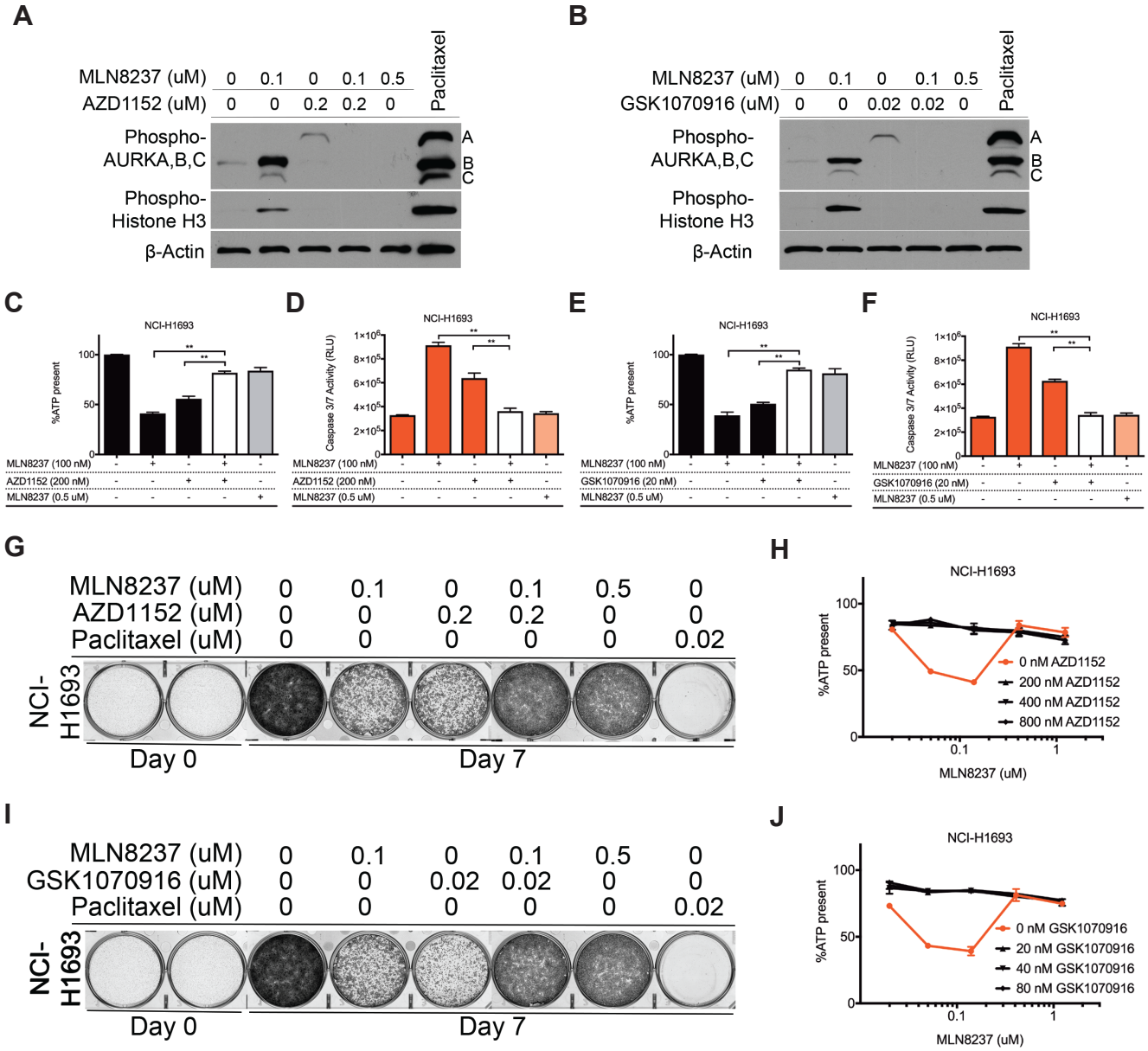
A
MLN8237 (uM) 0 0.1 0 0.1 0.5
AZD1152 (uM) 0 0 0.2 0.2 0
Paclitaxel
Phospho-AURKA,B,C
A
B
C
Phospho-Histone H3
β-Actin
B
MLN8237 (uM) 0 0.1 0 0.1 0.5
GSK1070916 (uM) 0 0 0.02 0.02 0
Paclitaxel
Phospho-AURKA,B,C
A
B
C
Phospho-Histone H3
β-Actin
C
NCI-H1693
%ATP present
MLN8237 (100 nM)
AZD1152 (200 nM)
MLN8237 (0.5 uM)
D
NCI-H1693
Caspase 3/7 Activity (RLU)
MLN8237 (100 nM)
AZD1152 (200 nM)
MLN8237 (0.5 uM)
E
NCI-H1693
%ATP present
MLN8237 (100 nM)
GSK1070916 (20 nM)
MLN8237 (0.5 uM)
F
NCI-H1693
Caspase 3/7 Activity (RLU)
MLN8237 (100 nM)
GSK1070916 (20 nM)
MLN8237 (0.5 uM)
G
MLN8237 (uM) 0 0.1 0 0.1 0.5 0
AZD1152 (uM) 0 0 0.2 0.2 0 0
Paclitaxel (uM) 0 0 0 0 0 0.02
NCI-H1693
Day 0
Day 7
H
NCI-H1693
%ATP present
0 nM AZD1152
200 nM AZD1152
400 nM AZD1152
800 nM AZD1152
MLN8237 (uM)
I
MLN8237 (uM) 0 0.1 0 0.1 0.5 0
GSK1070916 (uM) 0 0 0.02 0.02 0 0
Paclitaxel (uM) 0 0 0 0 0 0.02
NCI-H1693
Day 0
Day 7
J
NCI-H1693
%ATP present
0 nM GSK1070916
20 nM GSK1070916
40 nM GSK1070916
80 nM GSK1070916
MLN8237 (uM)

Figure 5

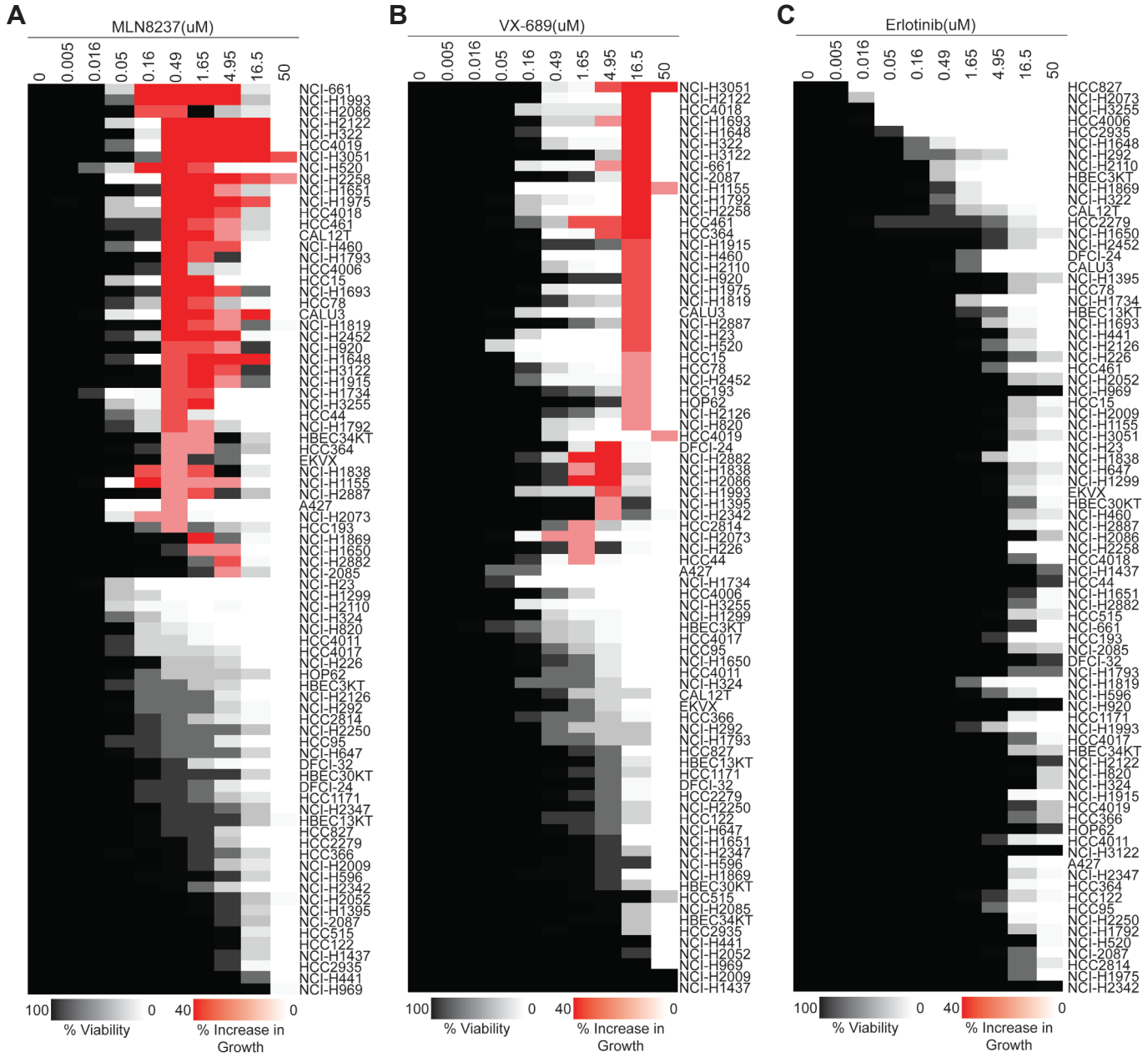
A
MLN8237(uM)
0
0.005
0.016
0.05
0.16
0.49
1.65
4.95
16.5
50
NCI-661
NCI-H1993
NCI-H2086
NCI-H2122
NCI-H322
HCC4019
NCI-H3051
NCI-H520
NCI-H2258
NCI-H1651
NCI-H1975
HCC4018
HCC461
CAL12T
NCI-H460
NCI-H1793
HCC4006
HCC15
NCI-H1693
HCC78
CALU3
NCI-H1819
NCI-H2452
NCI-H920
NCI-H1648
NCI-H3122
NCI-H1915
NCI-H1734
NCI-H3255
HCC44
NCI-H1792
HBEC34KT
HCC364
EKVX
NCI-H1838
NCI-H1155
NCI-H2887
A427
NCI-H2073
HCC193
NCI-H1869
NCI-H1650
NCI-H2882
NCI-2085
NCI-H23
NCI-H1299
NCI-H2110
NCI-H324
NCI-H820
HCC4011
HCC4017
NCI-H226
HOP62
HBEC3KT
NCI-H2126
NCI-H292
HCC2814
NCI-H2250
HCC95
NCI-H647
DFCI-32
HBEC30KT
DFCI-24
HCC1171
NCI-H2347
HBEC13KT
HCC827
HCC2279
HCC366
NCI-H2009
NCI-H596
NCI-H2342
NCI-H2052
NCI-H1395
NCI-2087
HCC515
HCC122
NCI-H1437
HCC2935
NCI-H441
NCI-H969
100
0
% Viability
40
0
% Increase in Growth
B
VX-689(uM)
0
0.005
0.016
0.05
0.16
0.49
1.65
4.95
16.5
50
NCI-H3051
NCI-H2122
HCC4018
NCI-H1693
NCI-H1648
NCI-H322
NCI-H3122
NCI-661
NCI-2087
NCI-H1155
NCI-H1792
NCI-H2258
HCC461
HCC364
NCI-H1915
NCI-H460
NCI-H2110
NCI-H920
NCI-H1975
NCI-H1819
CALU3
NCI-H2887
NCI-H23
NCI-H520
HCC15
HCC78
NCI-H2452
HCC193
HOP62
NCI-H2126
NCI-H820
HCC4019
DFCI-24
NCI-H2882
NCI-H1838
NCI-H2086
NCI-H1993
NCI-H1395
NCI-H2342
HCC2814
NCI-H2073
NCI-H226
HCC44
A427
NCI-H1734
HCC4006
NCI-H3255
NCI-H1299
HBEC3KT
HCC4017
HCC95
NCI-H1650
HCC4011
NCI-H324
CAL12T
EKVX
HCC366
NCI-H292
NCI-H1793
HCC827
HBEC13KT
HCC1171
DFCI-32
HCC2279
NCI-H2250
HCC122
NCI-H647
NCI-H1651
NCI-H2347
NCI-H596
NCI-H1869
HBEC30KT
HCC515
NCI-H2085
HBEC34KT
HCC2935
NCI-H441
NCI-H2052
NCI-H969
NCI-H2009
NCI-H1437
100
0
% Viability
40
0
% Increase in Growth
C
Erlotinib(uM)
0
0.005
0.016
0.05
0.16
0.49
1.65
4.95
16.5
50
HCC827
NCI-H2073
NCI-H3255
HCC4006
HCC2935
NCI-H1648
NCI-H292
NCI-H2110
HBEC3KT
NCI-H1869
NCI-H322
CAL12T
HCC2279
NCI-H1650
NCI-H2452
DFCI-24
CALU3
NCI-H1395
HCC78
NCI-H1734
HBEC13KT
NCI-H1693
NCI-H441
NCI-H2126
NCI-H226
HCC461
NCI-H2052
NCI-H969
HCC15
NCI-H2009
NCI-H1155
NCI-H3051
NCI-H23
NCI-H1838
NCI-H647
NCI-H1299
EKVX
HBEC30KT
NCI-H460
NCI-H2887
NCI-H2086
NCI-H2258
HCC4018
NCI-H1437
HCC44
NCI-H1651
NCI-H2882
HCC515
NCI-661
HCC193
NCI-2085
DFCI-32
NCI-H1793
NCI-H1819
NCI-H596
NCI-H920
HCC1171
NCI-H1993
HCC4017
HBEC34KT
NCI-H2122
NCI-H820
NCI-H324
NCI-H1915
HCC4019
HCC366
HOP62
HCC4011
NCI-H3122
A427
NCI-H2347
HCC364
HCC122
HCC95
NCI-H2250
NCI-H1792
NCI-H520
NCI-2087
HCC2814
NCI-H1975
NCI-H2342
100
0
% Viability
40
0
% Increase in Growth

Figure 6

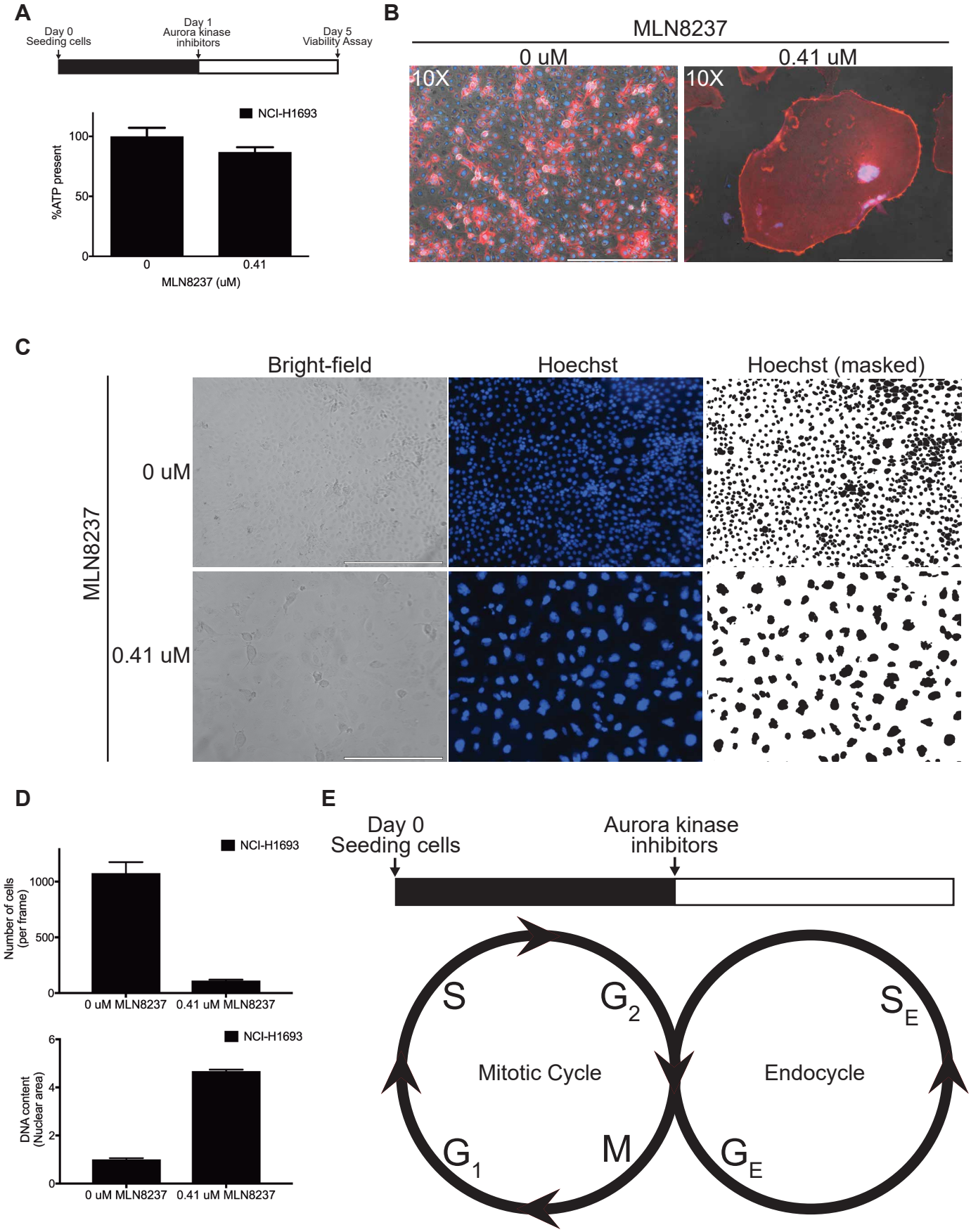
A
Day 0
Seeding cells
Day 1
Aurora kinase
inhibitors
Day 5
Viability Assay
NCI-H1693
%ATP present
100
50
0
0
0.41
MLN8237 (uM)
B
MLN8237
0 uM
0.41 uM
10X
10X
C
Bright-field
Hoechst
Hoechst (masked)
MLN8237
0 uM
0.41 uM
D
NCI-H1693
Number of cells
(per frame)
1000
500
0
0 uM MLN8237
0.41 uM MLN8237
NCI-H1693
DNA content
(Nuclear area)
6
4
2
0
0 uM MLN8237
0.41 uM MLN8237
E
Day 0
Seeding cells
Aurora kinase
inhibitors
S
G2
Mitotic Cycle
G1
M
SE
Endocycle
GE

Figure 7

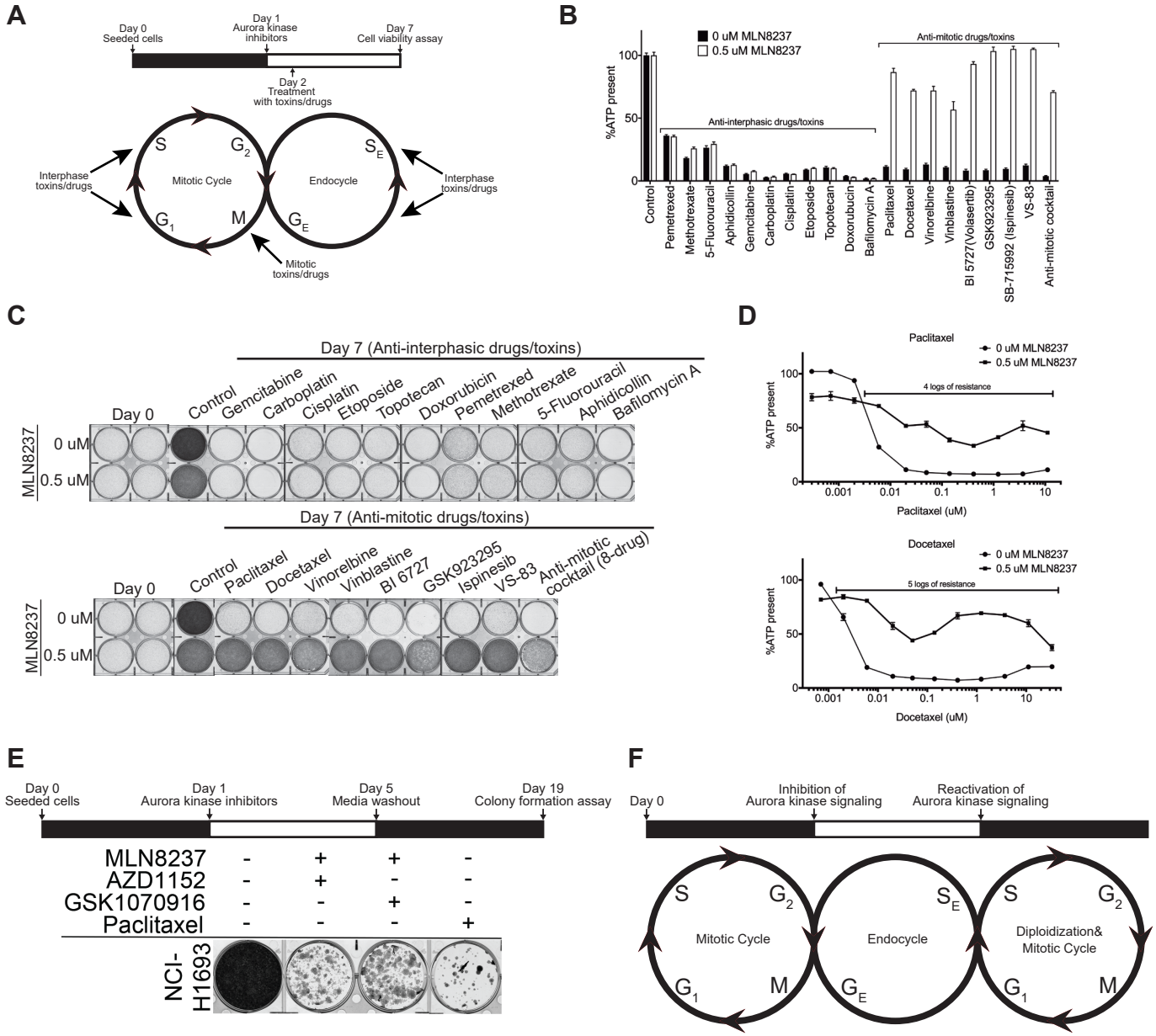
A
Day 0
Seeded cells
Day 1
Aurora kinase
inhibitors
Day 7
Cell viability assay
Day 2
Treatment
with toxins/drugs
S
G2
Mitotic Cycle
G1
M
SE
Endocycle
GE
Interphase
toxins/drugs
Interphase
toxins/drugs
Mitotic
toxins/drugs
B
0 uM MLN8237
0.5 uM MLN8237
%ATP present
Anti-interphasic drugs/toxins
Anti-mitotic drugs/toxins
Control
Pemetrexed
Methotrexate
5-Fluorouracil
Aphidicollin
Gemcitabine
Carboplatin
Cisplatin
Etoposide
Topotecan
Doxorubucin
Bafilomycin A
Paclitaxel
Docetaxel
Vinorelbine
Vinblastine
BI 5727(Volasertib)
GSK923295
SB-715992 (Ispinesib)
VS-83
Anti-mitotic cocktail
C
Day 7 (Anti-interphasic drugs/toxins)
Day 0
Control
Gemcitabine
Carboplatin
Cisplatin
Etoposide
Topotecan
Doxorubicin
Pemetrexed
Methotrexate
5-Fluorouracil
Aphidicollin
Bafilomycin A
MLN8237
0 uM
0.5 uM
Day 7 (Anti-mitotic drugs/toxins)
Day 0
Control
Paclitaxel
Docetaxel
Vinorelbine
Vinblastine
BI 6727
GSK923295
Ispinesib
VS-83
Anti-mitotic
cocktail (8-drug)
MLN8237
0 uM
0.5 uM
D
Paclitaxel
0 uM MLN8237
0.5 uM MLN8237
4 logs of resistance
%ATP present
Paclitaxel (uM)
Docetaxel
0 uM MLN8237
0.5 uM MLN8237
5 logs of resistance
%ATP present
Docetaxel (uM)
E
Day 0
Seeded cells
Day 1
Aurora kinase inhibitors
Day 5
Media washout
Day 19
Colony formation assay
MLN8237 - + + -
AZD1152 - + - -
GSK1070916 - - + -
Paclitaxel - - - +
NCI-H1693
F
Day 0
Inhibition of
Aurora kinase signaling
Reactivation of
Aurora kinase signaling
S
G2
Mitotic Cycle
G1
M
SE
Endocycle
GE
S
G2
Diploidization&
Mitotic Cycle
G1
M

Supplemental Figure 1

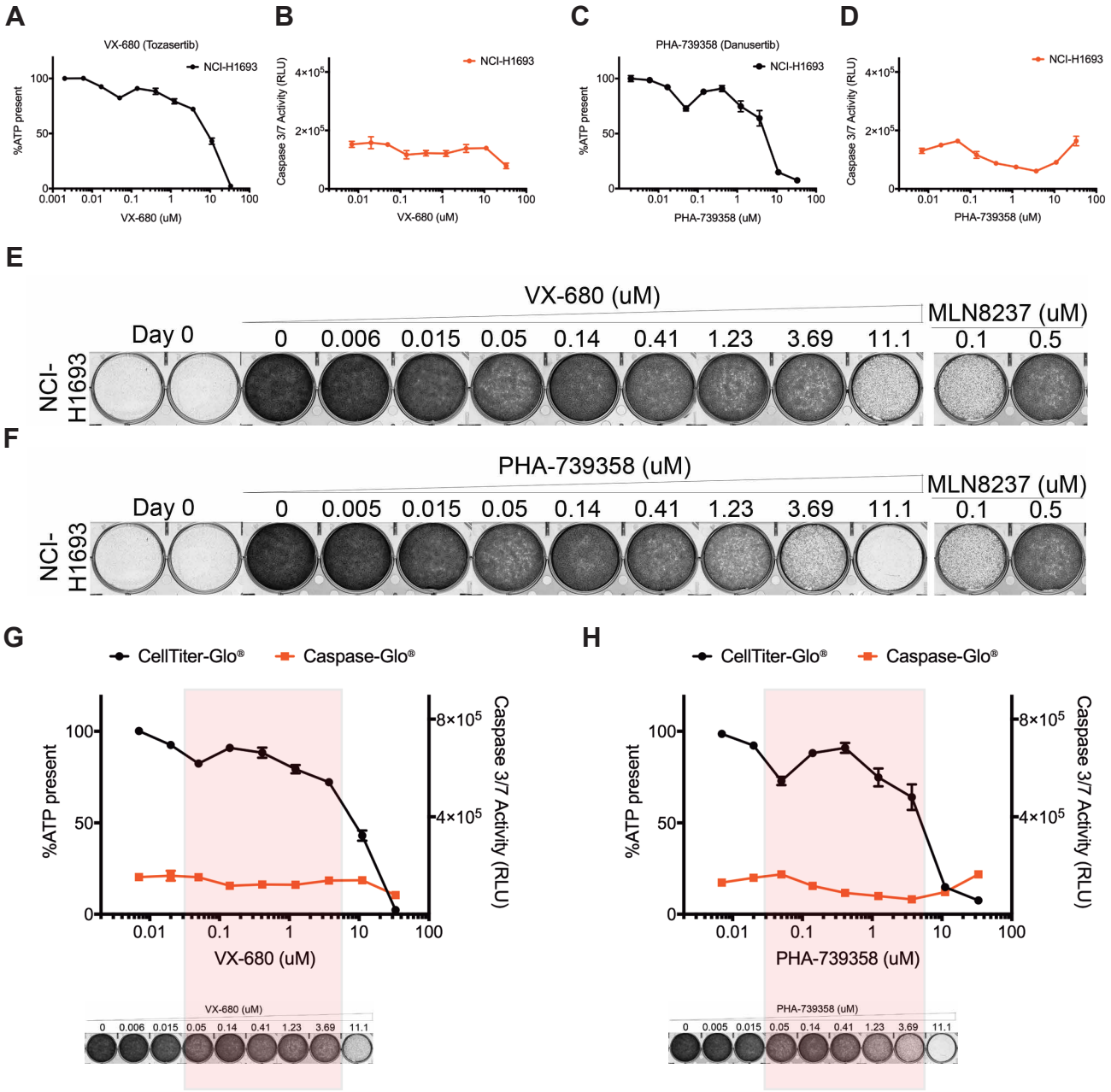
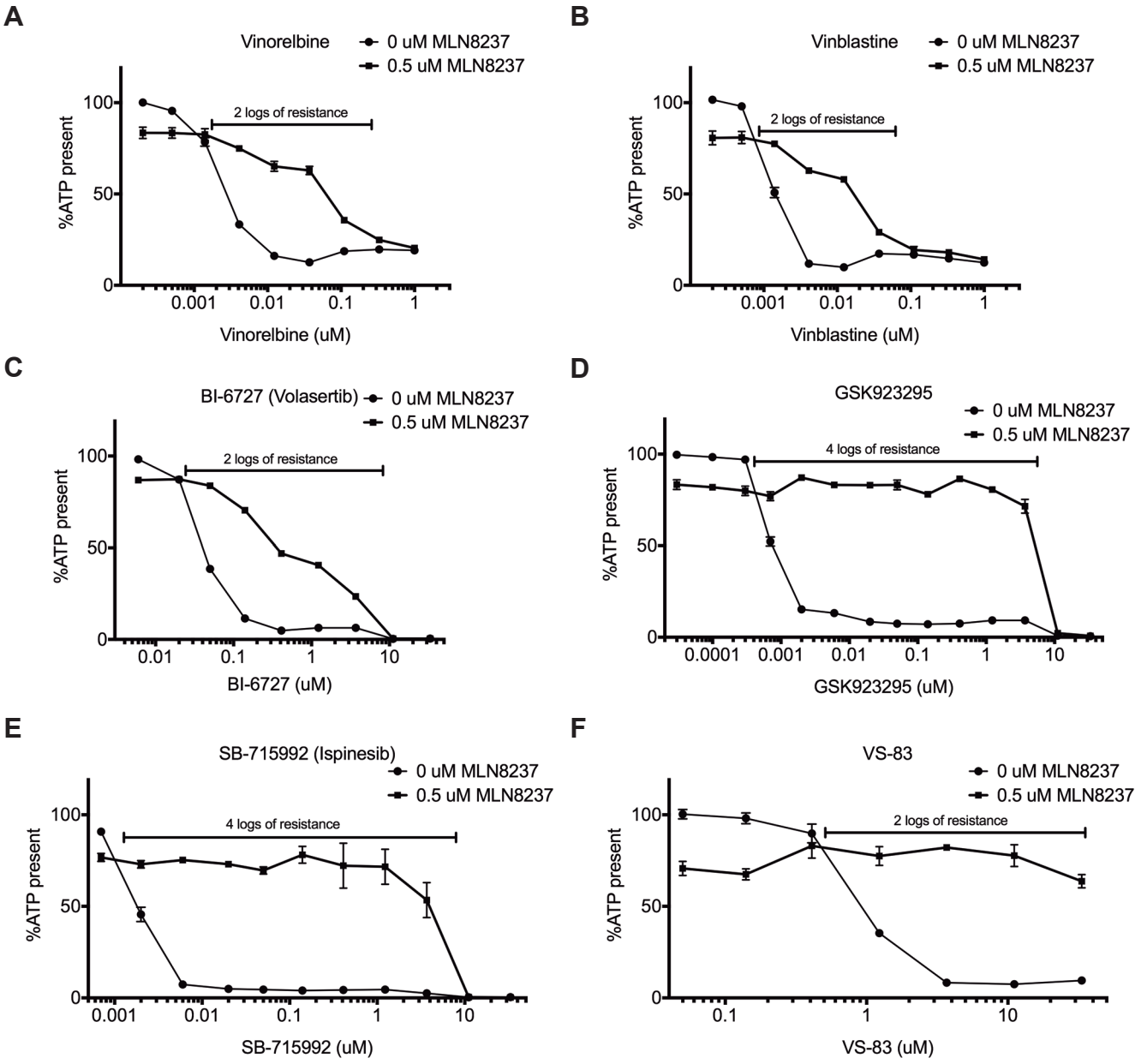
Supplemental Figure 2